In Situ Measurements of Aerosol Mass Concentration and Radiative Properties in Xianghe, SE of Beijing

Zahra Chaudhry[1,2], J. Vanderlei Martins[3,4], Zhanqing Li[1,2,5], Si-Chee Tsay[4], Hongbin Chen[5], Weidong Nan[5], Tianxue Wen[5], Can Li[1], Russell R. Dickerson[1]

1) Department of Atmospheric and Oceanic Science
University of Maryland
College Park, MD
2) Earth System Science Interdisciplinary Center
University of Maryland
College Park, MD
3) Department of Physics and Joint Center for Earth Systems and Technology
University of Maryland-Baltimore County
Baltimore, MD
4) NASA Goddard Space Flight Center
Greenbelt, MD
5) Institute of Atmospheric Physics
Chinese Academy of Sciences
Beijing, China

Submitted to

Journal of Geophysical Research-Atmosphere

A special issue on

**East Asian Study of Tropospheric Aerosols:
An International Regional Experiment**

(EAST-AIRE)

Abstract

As a part of the EAST-AIRE study, Nuclepore filters were collected in two size ranges (coarse, 2.5μm<d<10μm, and fine, d<2.5μm) from January-May 2005 in Xianghe, about 70 km southeast of Beijing and analyzed for aerosol mass concentration, spectral absorption efficiency and absorption coefficient. Twelve-hour aerosol mass concentration measurements showed an average concentration of 120 $\mu g/m^3$ in the coarse mode, and an average concentration of 25 $\mu g/m^3$ in the fine mode. To determine how representative ground-based measurements are of the total column, the mass concentration data was compared with AERONET AOT at 500nm and AERONET size distribution data. The vertical distribution of the aerosols were studied with a micro-pulse lidar and in the cases where the vertical column was found to be fairly homogenous, the comparisons of the filter results with AERONET agreed favorably, while in the cases of inhomogeneity, the comparisons have larger disagreement. For fine mode aerosols, the spectral absorption efficiency compares favorably to a λ^{-1} model, while the coarse mode shows a much flatter spectral dependence, consistent with large particle models. The coarse mode absorption efficiency was compatible with that of the fine mode in the NIR region, indicating the much stronger absorption of the coarse mode due to its composition and sizeable mass. Single scattering albedo results are presented from a combination between absorption coefficients derived from the filter measurements, from a PSAP and from a three-wavelength Nephelometer.

1. Introduction

According to the *IPCC* [2001], our ability to quantify the direct effect of aerosols on the global climate is hindered severely by large uncertainties in the measurements of aerosol absorption. Both the sign and magnitude of the forcing at the top of the atmosphere is dictated by aerosol absorption, loading and surface albedo [*Coakley and Chylek*, 1975]. Rarely are such pure aerosol types found in the atmosphere, as they are generally mixtures of different types, which further increases the complexity of quantifying the effect that aerosols have on local and regional climate [*Jacobson*, 2000]. Further knowledge is needed on both aerosol composition and vertical distribution.

Various instruments such as the Integrating Plate [*Lin et al.*, 1973], Particle/Soot Absorption Photometer (PSAP, Radiance Research, Seattle, WA), Aethalometer [*Hansen et al.,* 1983] and other filter-based measurements have been used to gain data on aerosol absorption. In cases where the vertical distribution of aerosols is fairly uniform, ground-based measurements are able to represent the optical properties of aerosols in the total column with little uncertainty. This is highly desirable as ground-based measurements are relatively easy to acquire, cost-effective and can offer good spatial and temporal resolution.

Remote sensing techniques such as satellites, lidar instruments and the Aerosol Robotic Network, AERONET [*Holben et al*., 1998], are better at measuring the total column of aerosols, and for gathering data on the vertical profile of aerosol optical properties. Passive satellite remote sensing also offers excellent spatial coverage, but depending on

87 the vertical structure of the atmosphere, it has problems providing the aerosol
88 concentration near the ground. Lidar measurements from space provide good assessment
89 of the vertical distribution of aerosols and clouds but have significantly less spatial
90 coverage than the passive instruments (eg. CALIPSO, *Winker et al.* [2003], GLAS,
91 *Zwally et al.* [2002]). The drawback of column mean values is that they can mean very
92 little to near-surface absorption if large concentrations of aerosols are aloft in higher
93 layers. Besides, collecting aerosol samples on the ground level also has advantage of
94 studying their impact on health as aerosols are a known health risk.
95
96 The rapid population and economic growth seen in China over the last few decades has
97 had strong effects on the local and regional air quality and climate. The increase in
98 manufacturing and demand for products has led to serious air quality concerns. Several
99 intensive studies have been conducted recently to examine the transport of air masses
100 from the region over the Pacific such as ACE-Asia [*Huebert et al*., 2003] and INTEX-
101 NA. EAST-AIRE takes a closer look at the physical, optical and chemical properties of
102 aerosols across China through a series of ground-based observation stations [*Z. Li et al*.,
103 this issue]. One particular site, Xianghe, was chosen to host an Intensive Observation
104 Campaign (IOC) during March 2005, when many instruments measuring the same
105 parameters were run side-by-side to calibrate newer instruments against well-used and
106 well-characterized instruments, as well as to ensure accurate measurements across
107 various levels of resolution. The measurement site is detailed in *C. Li et al*. [this issue].
108 For aerosol absorption, six instruments were run during this time period: 2 PSAPs, 3
109 Aethalometers and one sampling apparatus for collecting Nuclepore filters. This study

110 will examine results from the Nuclepore filters and compare its absorption results against
111 the University of Maryland's PSAP and the AERONET instrument.
112
113 While other measurements of aerosol absorption allow for higher temporal resolution, the
114 filter results allow for a more detailed spectral absorption analysis from 350-2500nm.
115 These results, in combination with the mass measurements, allow for the direct
116 determination of the spectral mass absorption efficiency (in m^2/g) and for the study of
117 individual particles using scanning electron microscopy. By collecting aerosol samples
118 for 12 hours, the day/night separation is preserved and the resulting Nuclepore filters
119 have enough loading to be submitted for additional chemical composition analysis, such
120 as ICPMS, PIXE or Ion Chromatography [*Ma et al*., 2001, *Yamasoe et al*., 2000].
121 Nuclepore filters offer a smooth surface for filter collection, preventing optical artifacts
122 encountered with other filter types such as paper, Teflon and quartz [*Weiss and*
123 *Waggoner*, 1984]. Particle collection on Nuclepore filters is also low-tech, using a
124 simple sampling train, making it low-cost and ideal for field experiments.
125
126 Other studies presented in this special issue address the issue of quantifying the aerosol
127 radiative properties in Xianghe [*Li et al*., this issue]. *Zhao and Li* use spectral direct
128 radiance measurements from an AERONET sunphotometer with total sky irradiance from
129 a pyranometer to retrieve the single-scattering albedo. Their advantage is higher
130 temporal resolution, on the order of 20 seconds, but they are limited to only cloud-free
131 conditions, which is not an issue in this study. *C. Li et al*. examines aerosol radiative
132 properties using a PSAP and a TSI three-wavelength Nephelometer, in association with

many precursor gases measurements. Data from *C. Li et al*. is used in this study as a comparison with the filter measurements, and for the calculation of the average single scattering albedo throughout the filter sampling period. While the PSAP provides higher temporal resolution data than collecting filters, no upper-end cut-off was used, possibly skewing the results with large particles.

In this study, we present results of five months of data sampling in Xianghe, China. Mass concentration measurements are presented in two size categories (coarse and fine) and compared with AERONET size distribution and AOT. The spectrally-dependent absorption efficiency is measured and the absorption coefficient is calculated.

2. Methodology

A two-stage sampling apparatus was installed at Xianghe, China in January, 2005 to collect aerosol particles on Nuclepore filters. The system has an impactor inlet ensuring a 10μm aerodynamic diameter cut-off size and the impactor was coated with Apiezon grease to reduce particle bounce. The first filter collected particles larger than 2.5μm (hereafter referred to as the coarse mode) and the second filter collected particles less than 2.5μm aerodynamic diameter (hereafter referred to as the fine mode). Size-resolved filters were collected twice daily up to and through the IOC (January-March) and collected once daily for the next two months (April and May), with a few breaks due to instrument or supply-related problems. From January through March, the filters were changed between 6-7am in the morning and between 7-8pm in the evening. The initial flow through the filters was set at 18 lpm manually and only filters with a final flow of

156 greater than 8 lpm were analyzed. The instantaneous flow rate was recorded in a data
157 logger and utilized in data analysis to correct for flow changes during the sampling.
158
159 The filters were subjected to gravimetric analysis prior to and after field deployment.
160 Blank filters were sent to the field amongst the exposed filters and were treated similarly
161 to monitor the whole process. The filters were exposed to an ionizer for 24 hours prior to
162 weighing to remove static charge and to ensure an accurate weight measurement. The
163 humidity in the ionizing chamber was recorded for each cycle and maintained around
164 20%. The humidity of the weighing room was also recorded at around 40%. The
165 difference in humidity was determined not to affect the particles on the filters. Since the
166 particle were collected at a variety of humidity levels, but analyzed dry, the higher
167 humidity of the weighing room was not great enough to rehumidify the particles.
168 According to meteorological data at the measurement site in Xianghe, the local humidity
169 level stayed relatively low, averaging 36% during the IOC [*C. Li et al.*, this issue].
170
171 After gravimetric analysis, the filters were subjected to an optical reflectance (OR)
172 technique previously applied in *Martins et al.* [1998], validated against an extinction cell
173 and Nephelometer measurements in *Reid et al.* [1998] and described in detail in *Martins*
174 *et al*. [2006]. Since the aerosol particles were collected on the surface of Nuclepore
175 filters, we expect less optical artifacts with this method than with particles collected
176 inside the fibers of quartz, Teflon or paper filters. The filter is placed on a diffusive
177 Spectralon panel and illuminated from above. The amount of light reflected is measured
178 from 350nm to 2500nm by an ASD (Analytical Spectral Devices) LabSpec Pro

179 spectrometer, with radiometric stability of 1% and precision of approximately 3% [*Kindel*
180 *et al*., 2001]. By passing light through the particles and reflecting the light off the filter
181 and the Lambertian surface below, we are essentially mimicking the same method used
182 by satellite sensors with the advantage that we can characterize well the bright surface
183 underneath the particles. Blank filters were also placed on top of the Spectralon panel
184 and measured as a reference for the reflectance method. A calibration curve using
185 artificial black carbon particles with known optical properties and a variety of mass
186 loading is presented in *Martins et al*. [2006].
187
188 The light attenuation by absorbing particles and the mass concentration are used to
189 determine the spectral absorption efficiency (m^2/g). The spectral absorption efficiency
190 can be combined with the mass concentration measurement ($\mu g/m^3$) to obtain the
191 absorption coefficient (m^{-1}). The absorption coefficient was calculated from the filters by
192 utilizing the OR absorption efficiency at 550nm and was compare with PSAP results at
193 574nm, which was operated in parallel with the filter sampling apparatus. The 550nm
194 wavelength was chosen to compare with the three-wavelength Nephelometer used during
195 the IOP. Data from the University of Maryland's PSAP was obtained corresponding to
196 the IOP at 5-minute intervals, corrected according to *Bond et al.* [1999], and extrapolated
197 to 550nm following *Virkkula et al.* [2005]. The University of Maryland's instruments are
198 detailed in *C. Li et* al. [this issue]. Since the filters were collected over approximately 12-
199 hour intervals, the PSAP data was averaged over the same time period as the
200 corresponding filter. The PSAP average was also weighted according to the flow through
201 the filter to account for the decrease in flow throughout the sampling period. This

procedure ensured that both instruments sampled the aerosols similarly. This same process of averaging and weighting was applied to data obtained from the University of Maryland's three-wavelength TSI Nephelometer. The Single Scattering Albedo (ω_0) was calculated using the absorption coefficient from the PSAP and from the OR and the scattering coefficient from the Nephelometer at 550nm. The PSAP and Nephelometer were deployed on the same observatory tower as the filter sampling apparatus, but they did not include an upper-limit cut-off size like the 10μm inlet used for the filters [*C. Li et al*., this issue].

3. Results and Discussion

3.1 Mass concentration

The mass concentration of the particles was determined by gravimetric analysis and by the measured air volume sampled in each filter. The mass concentration of the coarse particles (2.5μm<d<10μm) from January 13-May 24, 2005 is shown in figure 1a. During this time period, values ranged from 8 to 407 μg/m^3 in the coarse mode with an average concentration of 120 μg/m^3. The mass concentration of the fine particles (d<2.5μm) is shown in figure 1b, where the values ranged from 10 to 79 μg/m^3 with an average concentration of 25 μg/m^3. Other studies to measure aerosol mass concentration in China have found similar results. *Bergen et al*. [2001] measured daily mean PM2.5 concentrations of 136 μg/m^3 with a standard deviation of 48 μg/m^3 during one week in June 1999 in Beijing, which expectedly shows higher concentrations than at Xianghe, which is in a relatively rural location. Also in Beijing, *Ning et al*. [1996] measured total

suspended particle (TSP) concentrations of 320 μg/m^3 in the summer and 680 μg/m^3 in the winter during two years of measurements in 1986 and 1987. In another Chinese city, Shanghai, *Ye et al*. [2003] measured weekly PM2.5 mass concentrations ranging between 21 μg/m^3 and 147 μg/m^3 at two locations, with an annual average of 57.9 μg/m^3 and 61.4 μg/m^3 at each site, from March 1999 through February 2000. *Shi et al*. [2003] chose a suburban location, Nankou, a town 45km northwest of central Beijing to study mass concentration, similar to this study. The authors measured PM2.5 mass concentrations of 177 ± 53 μg/m^3 and PM10 mass concentrations of 334 ± 96 μg/m^3 during one week in March of 2001.

From the mass concentration data during the IOC, which were separated in 12 hour day and night samples, a 24-hour average was calculated for PM2.5 and PM10. For the filter results, PM10 is defined as the sum of the fine and coarse filter, which will account for all particles of d< 10μm. The 24-hour IOC PM10 and PM2.5 results are shown in figure 2. To place the data in perspective, they are compared with the US EPA National Ambient Air Quality Standards (NAAQS). The 24-hour average NAAQS limit for PM2.5 (35 μg/m^3) and for PM10 (150 μg/m^3) are shown in the plot. The PM2.5 limit was exceeded once during the IOC, at an average concentration of 35.4 μg/m^3 on March 10, 2005. The PM10 limit, however, was breached on 67% of the days of the IOC, and on those days, averaged 47% greater concentrations than the NAAQS limit. Over the five-month sampling period, the PM2.5 limit was exceeded 13% of the days, and the PM10 limit was exceeded 43% of the days. While PM10 is considered to be a lesser

health risk than PM2.5, the respiratory problems, the visibility reduction, and the weather and climate impacts that arise from high concentrations of PM10 are still a valid concern.

In addressing the aerosol radiative forcing of the climate and health issues related to aerosol pollution, a major challenge remains as to how well the total column-mean properties of the aerosol retrieved from the ground (e.g. AERONET, *Holben et al*. [1998], *Smirnov et al*. [2000], *Smirnov et al*. [2003]) or from satellites (e.g. MODIS, *Kaufman et al*. [1997], *Remer et al*. [2002], *Ichoku et al*. [2002], *Chu et al*. [2002]) represent the mass concentration measurements or other observed aerosol properties at the ground level, or vice versa. The answer to this question has very important implications on the monitoring of aerosols from space and important practical implications on the development of observation networks. The existence of aged versus fresh aerosol particles, or long-range transport of different aerosol types (e.g. dust transported over pollution aerosols), or any other source of inhomogeneity in the vertical aerosol distribution throughout the atmospheric column can affect this relationship. This possibility must be studied in different location and on a case by case basis.

One way to compare the ground-based filter measurements to total column remote sensing is to look at AERONET-based retrievals of aerosol particle size distribution. Note that the size distribution data from AERONET was derived from the almucantar and principal plane scans, while the direct sun measurement lends a more confident quantity, the Aerosol Optical Thickness (AOT). Due to the heavy aerosol loading at Xianghe, many more direct sun measurements were recorded than almucantar and principal planes.

Since the filter samples were collected in two size ranges, fine and coarse, a direct comparison between the Small Mode Ratio, SMR, can be performed between the filter results and the AERONET total column almucantar retrievals. The filter SMR is calculated by dividing the daytime fine mode mass concentration by the total (fine + coarse) daytime mass concentration. The AERONET SMR comes from integrating the AERONET volume size distributions up to 2.24μm diameter (the closest size bin constraint to 2.5μm), and dividing by the total volume up to 10μm diameter. The AERONET calculations assume the same mass density for the fine and coarse modes. Figure 3 shows a comparison between the SMR results of the filter versus AERONET. The 1:1 line indicated in the plot shows that there is one group of points with good agreement between both techniques and a second group (circled) where the AERONET results show consistently larger SMR, indicating smaller particles in the atmospheric column than near the ground.

For the circled data points, one would assume that there was an external factor that did not allow the ground-based measurements to accurately represent the total column, usually in the case of aerosol layers aloft or diurnal changes within a relatively calm boundary layer. To clarify this hypothesis, data was used from NASA's MPLnet as a micro-pulse lidar was located nearby. Lidar scans for the dates with good agreement between the filter SMR and AERONET SMR showed relatively uniform aerosol concentrations throughout the measurable vertical extent, as shown in figure 4a on March 13, 2005. The time-series of AOT from AERONET was laid over the corresponding scan time period to determine if lidar backscatter variations were related to aerosol loading,

294 not cloud contamination or sampling biases in AERONET due to selective cloud cover
295 during portions of the day. Lidar scans for dates with poor agreement between the SMRs
296 usually showed heavy aerosol layers aloft, or very inhomogeneous aerosol concentrations
297 throughout the boundary layer, as seen in figure 4b for one case on March 15 2005.
298 Based on these results, we can say that the SMR data gathered by ground-based
299 measurements are accurate representations of the total column in those instances when
300 the total column is well-mixed.
301
302 Assuming a constant mass extinction efficiency (m^2/g), one can determine how well the
303 AOT retrieved by an AERONET sunphotometer can represent the mass concentration
304 measured on the ground. *Smirnov et al*. [2000] offer a similar comparison from Barbados
305 studying transported Saharan dust. Only quality-assured AERONET level 2.0 daily
306 averages from the sunphotometer located in Xianghe were used for this comparison.
307 Since the sunphotometer computes AOT from its direct sun measurement, the daytime
308 filters were selected instead of 24-hour filters as the sunphotometer can only collect data
309 during daylight hours. In figure 5a, the fine mode mass concentration is compared to
310 AERONET AOT at 0.50 μm, while figure 5b shows a similar comparison with PM10
311 concentrations. This particular wavelength was chosen for consistency as it will be used
312 throughout this paper. With help from the SMR comparison, we can identify two distinct
313 paths taken by the data. The points surrounded by circles in figure 5a show cases where
314 the correlation in SMR were poor, while points in squares indicated dates when there is
315 no AERONET size distribution data available. This result serves as a guide to filter the
316 best cases in the intercomparison between AOT retrievals and mass measurements. The

317 resulting points (without the circled/squared points) present a better correlation between
318 the AOT versus PM2.5 mass and provide a correlation coefficient of $R^2 = 0.84$, slope =
319 0.011 and intercept = -0.011. For the PM10 comparison, we present a correlation
320 coefficient of $R^2 = 0.67$, slope = 0.0017 and intercept = 0.056. Comparable to this PM10
321 correlation, *Smirnov et al*. [2000] reported a correlation coefficient of $R^2 = 0.71$, slope =
322 0.0036 and intercept = 0.082 for daily filters from a high volume bulk sampler and daily
323 average AOT measurements at 870nm from AERONET of the Saharan dust. They were
324 able to improve the correlation to $R^2 = 0.93$ by presenting their 2.5-year data set as one-
325 month averages.
326
327 **3.2 Absorption efficiency**
328 The absorption efficiency is an important variable connecting the aerosol absorption
329 properties and the aerosol particle mass concentration and can be used in chemical
330 transport models to connect chemistry and optical properties. The absorption efficiency
331 is measured from the exposed Nuclepore filter using an optical reflectance technique and
332 the mass measurements [*Martins et al*., 2006]. The spectral dependence data provides
333 important information on the average size of the absorbers, and some hints on the
334 imaginary refractive index [*Martins et al.*, 1998]. In figure 6a, the absorption efficiency
335 of the coarse mode filters is shown as an average and one standard deviation of the 35
336 filters that were collected during the IOP. A second line is plotted showing a λ^{-1} spectral
337 dependence that is consistent with small absorbers, usually smaller than 0.2 μm diameter
338 and flat imaginary refractive index, like black carbon [*Martins et al*., 1998, *Bergstrom et*
339 *al*., 2002]. The absorption efficiency of the coarse mode has a much flatter spectral

dependence than the λ^{-1} line, which is consistent with larger particles with flat refractive index possibly representing large black carbon cluster aggregates or combinations between dust particles and black carbon [*Martins et al*., 1998]. However, the fine mode filters absorption efficiency is very similar to the λ^{-1} model, as shown in figure 6b. Departures from the λ^{-1} curve for small absorbing particles can be related to relatively fast changes in the imaginary component of the refractive index which is commonly observed in the short visible and the UV for organic materials [*Chang and Charalampopoulos*, 1990] or even dust.

The fine and coarse mode absorption efficiencies are compared side-by-side in figure 6c. While the fine mode is a more efficient absorber in the UV and visible regions, the fact that both modes are equally good absorbers, indicated by the overlapping error bars, in the near-IR is very important. Much of the incoming solar radiation is absorbed in this region of the spectrum, and since the coarse mode mass is much greater than that of the fine (figure 1a, b), the large absorption by the coarse mode is significant and is rarely taken into account in climate studies.

The typical fine and coarse particles collected in Xianghe during the IOP were observed by the use of a Scanning Electron Microscope on sections of the filter. Pictures were taken of several filters with the scanning electron microscope at the NASA Goddard Space Flight Center in Greenbelt, MD. Figure 7a shows an example for the filter collected on March 10th, where the fine-mode filter shows a combination of spherical particles and aggregates of much smaller particles. The black circles represent the filter

363 pores while the particles are pictured in shades of white and gray. The 1μm scale on the
364 bottom left corner indicates that all particles are smaller than 2.5 μm. The coarse mode
365 filter SEM in Figure 7b shows large particles probably composed of a combination of
366 dust, black carbon, and organic material from March 12. The mixture between dust and
367 black carbon could justify some of the absorption efficiency spectral dependence
368 observed in figure 6a and discussed in more details in *Martins et al*. [2006].
369
370 The absorption coefficient calculated from a combination of the OR and the mass
371 concentration was compared to the University of Maryland's PSAP instrument, which
372 was run in parallel with the filter sampling apparatus during the IOP. The comparison is
373 shown in figure 8. There is a better agreement between the two experimental techniques
374 at lower values of the absorption coefficient, while the disparity between the data points
375 widens at higher values probably due to biases of the PSAP corrections for higher
376 loading, and the excessive light attenuation allowed for those cases which could have
377 produced transmittances down to 60%. At seven points the difference between the two
378 measurements is greater than ±1E-05. The points where the OR measures a significantly
379 greater absorption coefficient (March 7th, March 14th, and March 19th) were all during the
380 night-time sampling period when the PSAP has difficulty taking continuous
381 measurements (see below for discussion). The largest difference of two points occurs
382 over the whole day of March 16th ending on March 17th when there was heavy
383 atmospheric loading based on Figure 2.
384

385 Using the scattering coefficient from The University of Maryland's TSI three-wavelength
386 Nephelometer, the SSA (ω_0) was calculated for both the filter OR and the PSAP results.
387 While the absorption coefficient can be derived from the OR measurement at any
388 wavelength from 350-2500μm, the Nephelometer only measures at 450, 550 and 700 nm.
389 The ω_0 was calculated at these three wavelengths and is shown in figure 9. The PSAP
390 only operates at one wavelength, 574nm. The filter OR ω_0 calculation at 550nm is then
391 compared with that from the PSAP (extrapolated from 574nm to 550nm), and
392 AERONET at 441nm and 673nm in figure 10. The ω_0 from AERONET is an inversion
393 product derived from almucantar and principle plane measurements, not direct sun
394 measurements, hence having fewer data points. To allow for some comparison, all data
395 points during this time period are shown, not just daily averages. The data shows that
396 AERONET's ω_0 is higher than that obtained from the ground-based measurements.
397 AERONET's inversion-based calculation would be influenced by aerosol layers aloft or
398 possibly by hydration of the ambient aerosol particles, neither of which would affect the
399 dry filter samples collected at the surface and analyzed in the lab.
400
401 Since the PSAP and Nephelometer instruments offer higher temporal resolution than OR,
402 we examined the diurnal cycle of ω_0 to determine whether or not the larger averaging
403 time would impact the findings. In figure 11, the daily cycle of ω_0 is shown with one
404 standard deviation at each data point. Also plotted on the top is the number of data points
405 that contributed to each average from the PSAP instrument. Since the PSAP is a filter-
406 based instrument using paper filters, the absorption measurement is only valid until a
407 certain threshold of loading on the filter, at which time the filter must be replaced. In the

408 case when an operator was not able to change the filter and the threshold was breached,
409 that data removed from the data set. The number of data points that contributed to each
410 average point gives us an idea of certainty in the measurement. The diurnal cycle of ω_0
411 shows two minima values corresponding to the rush hours of the morning and evening.
412

413 **4 Conclusions**
414

415 Nuclepore filters were collected in Xianghe, China for the first 5 months of 2005. Mass
416 concentration measurements derived from the filters indicate substantial atmospheric
417 loading of both PM2.5 and PM10. The ground-based mass concentration measurements
418 compare favorably with AERONET AOT and size distribution retrievals in cases of
419 vertical homogeneity as observed by the lidar data, which allows for converting
420 remotely-sensed AOT to mass concentration. The spectral absorption efficiency was
421 measured for the coarse and fine mode filters using an optical reflectance technique. The
422 fine mode compared favorably to a λ^{-1} model while the coarse mode exhibited much
423 flatter spectral dependence, consistent with large particle models. The coarse mode
424 absorption efficiency in the NIR region was determined to be similar in strength to the
425 fine mode. This implies very strong absorption by the coarse mode, considering the
426 sizeable mass of coarse particles in the atmosphere, which is very important for the
427 energy balance of the atmosphere considering that much of the incoming solar radiation
428 is present in this region of the spectrum. The large absorption observed by the coarse
429 mode during this experiment is very significant and should be emphasized in future
430 studies as it is rarely taken into account in climate studies.

The absorption coefficient was calculated at 550nm from the OR technique and compared to a co-located PSAP. At low to moderate levels of loading, the two measurement techniques compared very well, while the disparity increased at higher loading levels, probably due to the optical artifacts in the PSAP as well as few nighttime measurements. The absorption coefficients were combined with the scattering coefficient from a co-located Nephelometer to produce ω_0. Both ground-based measurements produced a lower ω_0 than AERONET, implying higher concentration of absorbers near the surface than aloft, or other intrinsic differences between the dry filter samples and the ambient measurements collected by AERONET. Such information is important to compute the temperature profile due to adiabatic heating by the aerosols. In the future, we plan to conduct more experiments using either airborne or balloon-borne instruments to better resolve the vertical profile of ω_0.

Acknowledgements: The EAST-AIRE project was supported by the NASA Radiation Science Program (NNG04GE79G), the National Science Foundation (ATM0412040, ATM425069), the National Science Foundation of China (40250120071), and the 973 Aerosol Initiative sponsored by the Chinese Ministry of Science and Technology. The absorption measurements were supported by the NASA Radiation Science Program. The authors would like to thank Jacob Kleidman for his filter/OR laboratory assistance, Debbie Thomas from NASA GSFC code 541.0 for her support on the SEM laboratory analysis.

5 References

Bergstrom, R.W, P.B. Russell, and P. Hignett (2002), Wavelength dependence of the absorption of black carbon particles: predictions and results from the TARFOX experiment and implications for the aerosol single scattering albedo, *J. Atmos. Sci.*, *59*, 567-577.

Bond, T.C., T.L. Anderson, and D. Campbell (1999), Calibration and intercomparison of filter-based measurements of visible light absorption by aerosols, *Aerosol Sci. Technol*., *30*, 582-600.

Campbell, D., S. Copeland, T. Cahill, R. Eldred, C. Cahill, and J. Vesenka (1989), The coefficient of optical absorption from particles deposited on filters: Integrating plate, Integrating sphere, and coefficient of haze measurements, Presented at the Annual Meeting of the AWMA.

Chang, H. and T.T. Charalampopoulos (1990), Determination of the wavelength dependence of refractive indices of flame soot, *Proceedings of The Royal Society of London: Mathematical and Physical Sciences*, *430*, 577-591.

Chu, D.A., Y.J. Kaufman, C. Ichoku, L.A. Remer, D. Tanre, and B.N. Holben (2002), Validation of MODIS aerosol optical depth retrieval over land, *Geophys. Res. Lett*., *29*, MOD2-1-4.

Coakley, J.A and P. Chylek (1975), The two-stream approximation in radiative transfer: Including the angle of incident radiation, *J. Atmos. Sci.*, *32(2*).

Hansen, A.D.A, H. Rosen, and T. Novakov (1983), Aethalometer: An instrument for the real-time measurement of optical absorption by aerosol particles, Presented at the 2nd

International Conference on Carbonaceous Particles in the Atmosphere, Linz, Austria, Sept. 11-14.

Holben, B.N. et al. (1998), AERONET- A federated instrument network and data archive for aerosol characterization, *Remote Sens. Environ.*, *661(1)*, 1-16.

Huebert, B.J., T. Bates, P.B. Russell, G. Shi, Y.J. Kim, K. Kawamura, G. Carmichael, and T. Nakajima (2003), An overview of ACE-Asia: Strategies for quantifying the relationships between Asian aerosols and their climatic impacts, *J. Geophys. Res.*, *108(D23),* ACE1-1.

Ichoku, C., D.A. Chu, S. Mattoo, Y.J. Kaufman, L.A. Remer, D. Tanre, I. Slutsker, and B.N. Holben (2002), A spatio-temporal approach for global validation and analysis of MODIS aerosol products, *Geophys. Res. Lett.*, *29*, MOD1-1-4.

Intergovernmental Panel on Climate Change (2001), *Climate Change 2001: The Scientific Basis*, Edited by J.T. Houghton, 896 pp., Cambridge University Press, New York.

Jacobson, M.Z. (2000), A physically-based treatment of elemental carbon optics: Implications for global direct forcing of aerosols, *Geophys. Res. Lett.*, *27*, 217-220.

Kaufman, Y.J., D. Tanre, L.A. Remer, E.F. Vermote, D.A. Chu, and B.N. Holben (1997), Operational remote sensing of tropospheric aerosol over land from EOS moderate resolution imaging spectroradiometer, *J. Geophys. Res.*, *102*, 17051-17067.

Kindel, B.C., Z. Qu, and A.F.H. Goetz (2001), Direct solar spectral irradiance and transmittance measurements from 350 to 2500nm, *Appl. Opt.*, *40(21)*, 3483-3494.

Lin, C.I., M. Baker, and R.J. Charlson (1973), Absorption coefficient of atmospheric aerosol: a method for measurement, *Appl. Opt.*, *12(6)*, 1356-1363.

500 Ma, C.-J., M. Kasahara, R. Holler, and T. Kamiya (2001), Characteristics of single
501 particles sampled in Japan during the Asian dust-storm period, *Atmos. Environ.*, *35*,
502 2707-2714.
503 Martins, J.V., P. Artaxo, C. Liousse, J.S. Reid, P.V. Hobbs, and Y.J. Kaufman (1998),
504 Effects of black carbon content, particle size, and mixing on light absorption by aerosols
505 from biomass burning in Brazil, *J. Geophys. Res.*, SCAR-B Special Issue, *103(D24)*,
506 32041-050.
507 Martins, J.V., P. Artaxo, Y. Kaufman, and A.D. Castanho (2006), Spectral absorption
508 properties of urban aerosol particles, In Preparation.
509 Ning, D., L. Zhong, and Y. Chung (1996), Aerosol size distribution and elemental
510 composition in urban areas of northern China, *Atmos. Environ.*, *30*, 2355-2362.
511 Reid, J.S., P.V. Hobbs, C. Liousse, J.V. Martins, R.E. Weiss, and T.F. Eck (1998),
512 Comparison of techniques for measuring shortwave absorption and black carbon content
513 of aerosols from biomass burning in Brazil, *J. Geophys. Res.*, SCAR-B Special Issue,
514 *103(D24)*, 32031-040.
515 Remer, L.A. et al. (2002), Validation of MODIS aerosol retrieval over ocean,
516 *Geophys. Res. Lett.*, *29*, MOD3-1-4.
517 Shi, Z., L. Shao, T.P. Jones, A.G. Whittaker, S. Lu, K.A. Berube, T. He, and R.J.
518 Richards (2003), Characterization of airborne individual particles collected in an urban
519 area, a satellite city and a clean air area in Beijing, 2001, *Atmos. Environ.*, *37*, 4097-4108.
520 Smirnov, A., B.N. Holben, D. Savoie, J.M. Prospero, Y.J. Kaufman, D. Tanre, T.F.
521 Eck, and I. Slutsker (2000), Relationship between column aerosol optical thickness and in
522 situ ground based dust concentrations over Barbados, *Geophys. Res. Lett.*, *27*, 1643-1646.

523 Virkkula, A., N.C. Ahlquist, D.S. Covert, W.P. Arnott, P.J. Sheridan, P.K. Quinn, and
524 D.J. Coffman (2005), Modification, calibration and a field test of an instrument for
525 measuring light absorption by particles, *Aerosol Sci. Technol.*, *39*, 68-83.
526 Weiss, R., and A. Waggoner (1984), Aerosol optical absorption: accuracy of filter
527 measurement by comparison with in-situ extinction, *Aerosols*, Edited by B. Liu, D. Pui,
528 and H. Fissan, pp 397.
529 Winker, D.M., J.R. Pelon, and M.P. McCormick (2003), The CALIPSO mission:
530 spaceborne lidar for observation of aerosols and clouds, *Proceedings of SPIE*, *4893*, 1-11.
531 Yamasoe, M.A., P. Artaxo, A.H. Miguel, and A.G. Allen (2000), Chemical
532 composition of aerosol particles from direct emissions of vegetation fires in the Amazon
533 Basin: Water-soluble species and trace elements, *Atmos. Environ.*, *34*, 1641-1653.
534 Ye, B., X. Ji, H. Yang, X. Yao, C.K. Chan, S.H. Cadle, T. Chan, and P.A. Mulawa
535 (2003), Concentration and chemical composition of PM2.5 in Shanghai for a 1-year
536 period, *Atmos. Environ.*, *37*, 499-510.
537 Zwally, H.J. et al. (2002), ICESat's laser measurements of polar ice, atmosphere,
538 ocean, and land, *J. Geodynamics*, *34*, 405-445.

539 Figure Captions
540
541 Figure 1. Twelve-hour Mass Concentration of a) coarse mode particles with aerodynamic
542 diameter 2.5μm<d<10μm, and b) fine mode particles with d<2.5μm for the period
543 between January 13-May 24, 2005 in Xianghe, China.
544
545 Figure 2. Twenty-four hour averages of PM2.5 (light gray) and PM10 (total column)
546 during the Intensive Observation Campaign compared to the US NAAQS 24-hour limit
547 for particulate matter.
548
549 Figure 3. Comparison between calculated AERONET Small Mode Ratio versus the
550 measured filter Small Mode Ratio for available data from January 13-May 24, 2005.
551 AERONET results were calculated from the average of almucantar inversions performed
552 throughout the day, whereas the filter data was sampled during the daylight hours. The
553 1:1 line is shown in the plot to indicate cases of good agreement between both results.
554 Cases of poorer agreement are circled.
555
556 Figure 4. Lidar scan and corresponding AOD time series from AERONET for a) March
557 13, 2005, representing one case when the calculated AERONET Small Mode Ratio
558 (SMR) and the filter SMR were correlated. The panel shows a relatively well-mixed
559 boundary layer during the AERONET data collection and the filter sampling period.
560 Panel b) March 15, 2005, represents one case when the calculated AERONET SMR and
561 the filter SMR did not correlate well and the lidar image shows significantly
562 heterogeneous layers during the sampling period.
563
564 Figure 5. a) Fine mode and b) PM10 concentrations versus AERONET AOT at 500nm.
565 The marked points are not included in the correlation; circled points indicate lack of
566 agreement from the SMR comparison in figure 3 while squared points indicate lack of
567 AERONET size distribution data.
568
569 Figure 6. Spectral Absorption Efficiency for aerosol particles of a) 2.5μm<d<10μm and
570 b) d<2.5μm averaged from 35 filters from March 3-19, 2005 compared to a λ^{-1} model,
571 then compared to each other in c. The gray area in each case represents the standard
572 deviation of the measured cases. The error bars in figure c is equivalent to the gray areas
573 in the figure a plot, but is shown as error bars for visual clarity.
574
575 Figure 7. Scanning Electron Microscope image of a) March 10, 2005 fine mode filter and
576 b) March 12, 2005 coarse mode filter. The scale in figure a corresponds to 1μm and the
577 scale in figure b corresponds to 2μm. The black circles shown are the filter pores
578 whereas the particles are shown in white and gray tones.
579
580 Figure 8. Comparison of absorption coefficient from the Optical Reflectance (OR)
581 technique applied to the Nuclepore filters and the corresponding average PSAP results
582 during the IOP.
583

584 Figure 9. Single Scattering Albedo (ω_0) from Optical Reflectance combined with the
585 Nephelometer scattering coefficient at the three operating wavelengths: 450, 550, 700nm.
586
587 Figure 10. Single Scattering Albedo from AERONET and a combination of the scattering
588 coefficient from the Nephelometer at 550nm with Optical Reflectance and PSAP results.
589
590 Figure 11. Diurnal cycle of Single Scattering Albedo from PSAP and Nephelometer with
591 error bars (light gray) and the number of data points from PSAP contributing to the
592 average (squares).
593

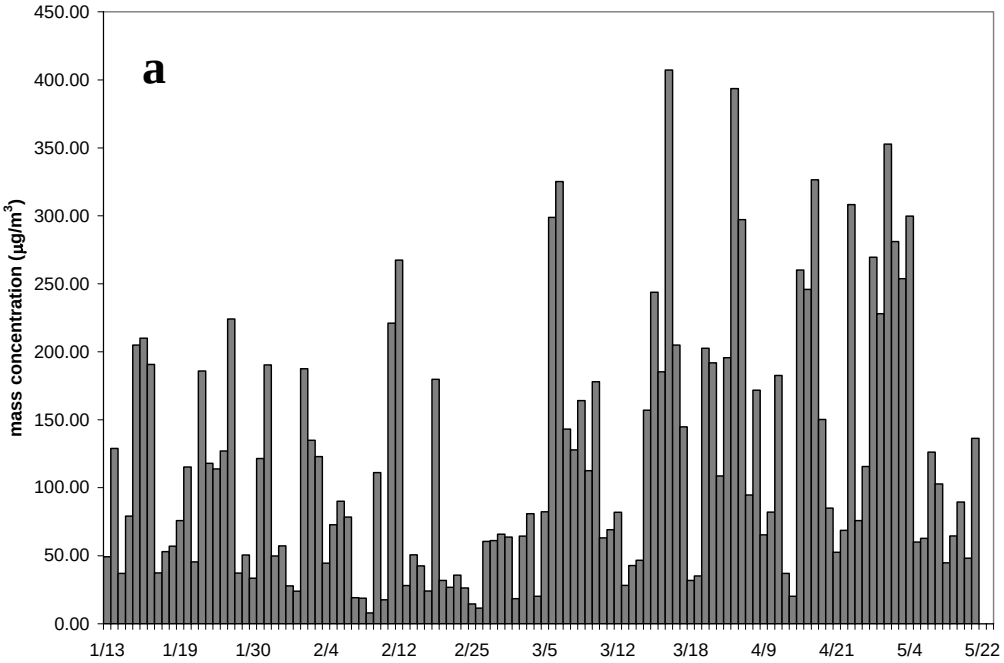

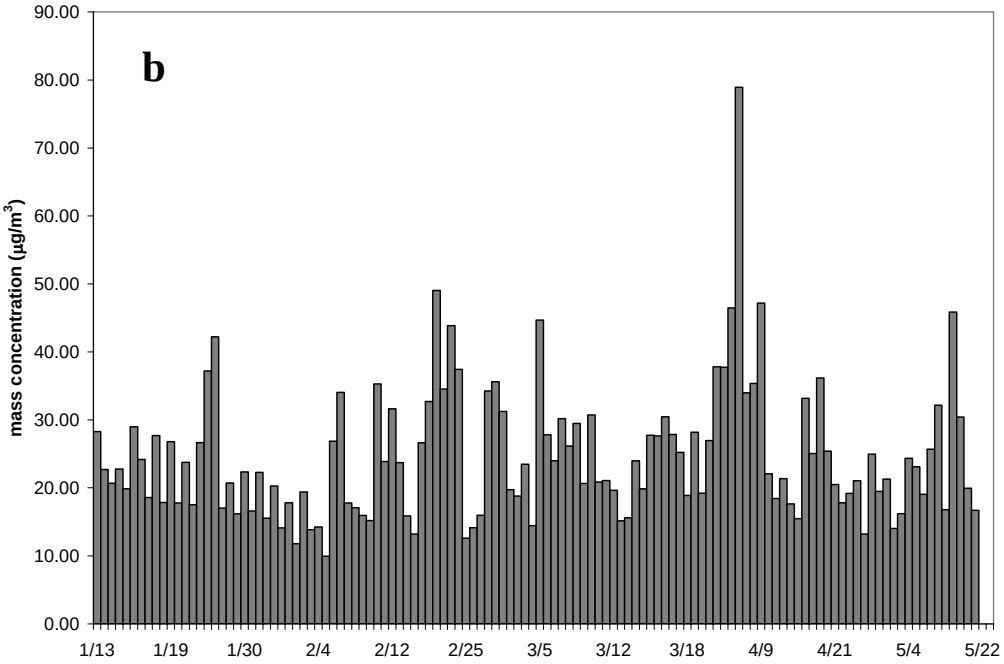

Figure 1. Twelve-hour Mass Concentration of a) coarse mode particles with aerodynamic diameter 2.5μm<d<10μm, and b) fine mode particles with d<2.5μm for the period between January 13-May 24, 2005 in Xianghe, China.

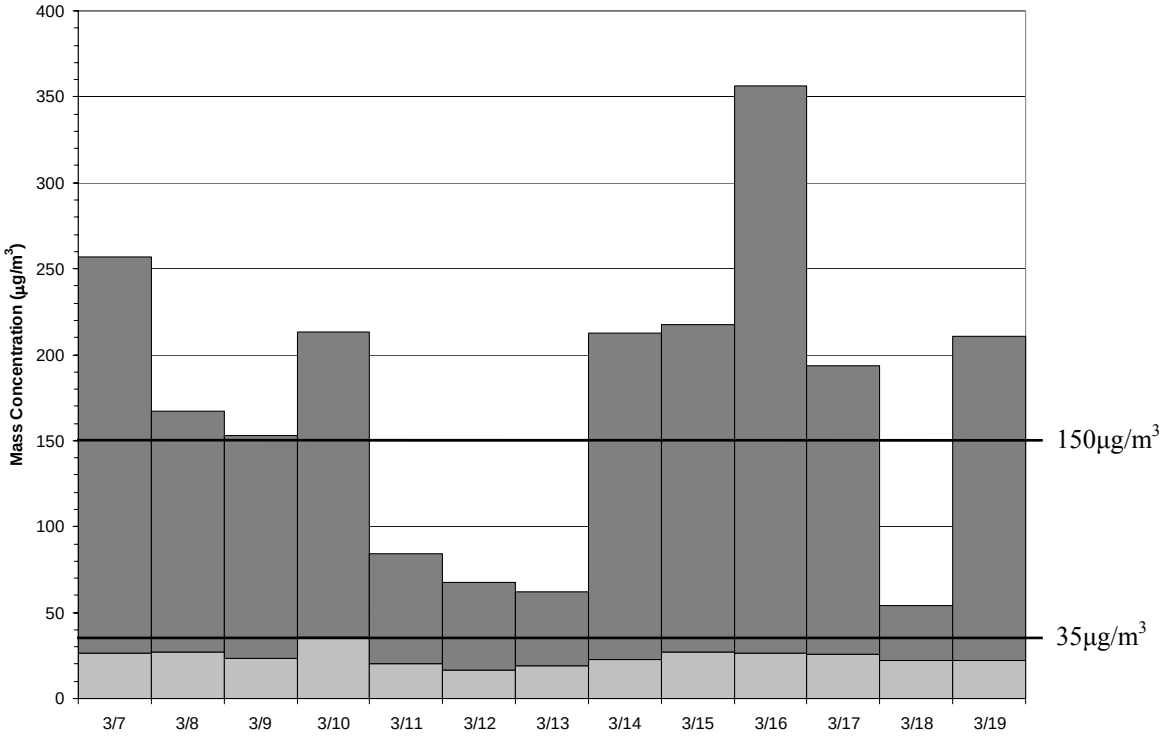

600

601 Figure 2. Twenty-four hour averages of PM2.5 (light gray) and PM10 (total column)

602 during the Intensive Observation Campaign compared to the US NAAQS 24-hour limit

603 for particulate matter.

604

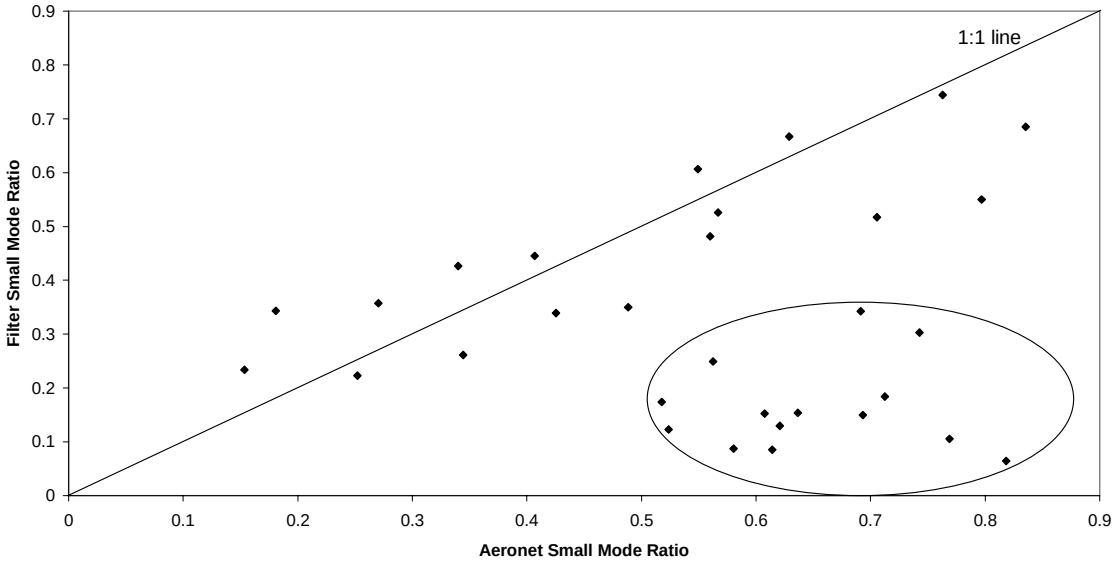

605

606 Figure 3. Comparison between calculated AERONET Small Mode Ratio versus the
607 measured filter Small Mode Ratio for available data from January 13-May 24, 2005.
608 AERONET results were calculated from the average of almucantar inversions performed
609 throughout the day, whereas the filter data was sampled during the daylight hours. The
610 1:1 line is shown in the plot to indicate cases of good agreement between both results.
611 Cases of poorer agreement are circled.

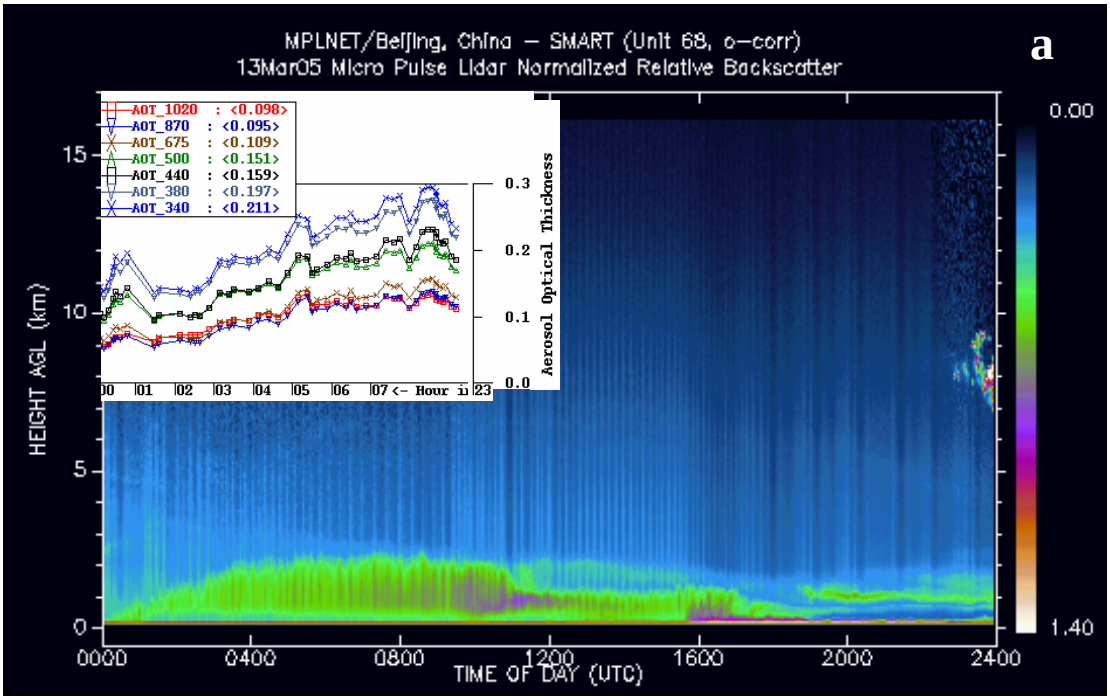
MPLNET/Beijing, China – SMART (Unit 68, c–corr)
13Mar05 Micro Pulse Lidar Normalized Relative Backscatter
a
AOT_1020 : <0.098>
AOT_870 : <0.095>
AOT_675 : <0.109>
AOT_500 : <0.151>
AOT_440 : <0.159>
AOT_380 : <0.197>
AOT_340 : <0.211>
Aerosol Optical Thickness
HEIGHT AGL (km)
TIME OF DAY (UTC)
0.00
1.40

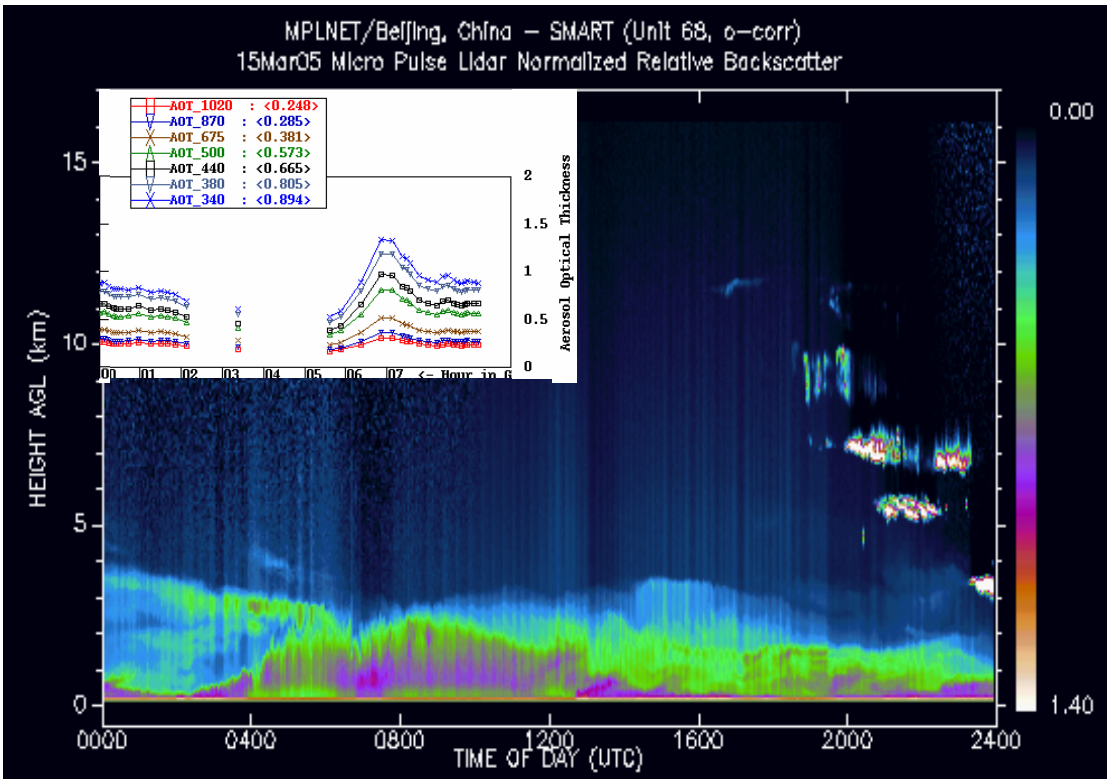
MPLNET/Beijing, China – SMART (Unit 68, c–corr)
15Mar05 Micro Pulse Lidar Normalized Relative Backscatter
AOT_1020 : <0.248>
AOT_870 : <0.285>
AOT_675 : <0.381>
AOT_500 : <0.573>
AOT_440 : <0.665>
AOT_380 : <0.805>
AOT_340 : <0.894>
Aerosol Optical Thickness
HEIGHT AGL (km)
TIME OF DAY (UTC)
0.00
1.40

612

Figure 4. Lidar scan and corresponding AOD time series from AERONET for a) March 13, 2005, representing one case when the calculated AERONET Small Mode Ratio (SMR) and the filter SMR were correlated. The panel shows a relatively well-mixed boundary layer during the AERONET data collection and the filter sampling period. Panel b) March 15, 2005, represents one case when the calculated AERONET SMR and the filter SMR did not correlate well and the lidar image shows significantly heterogeneous layers during the sampling period.

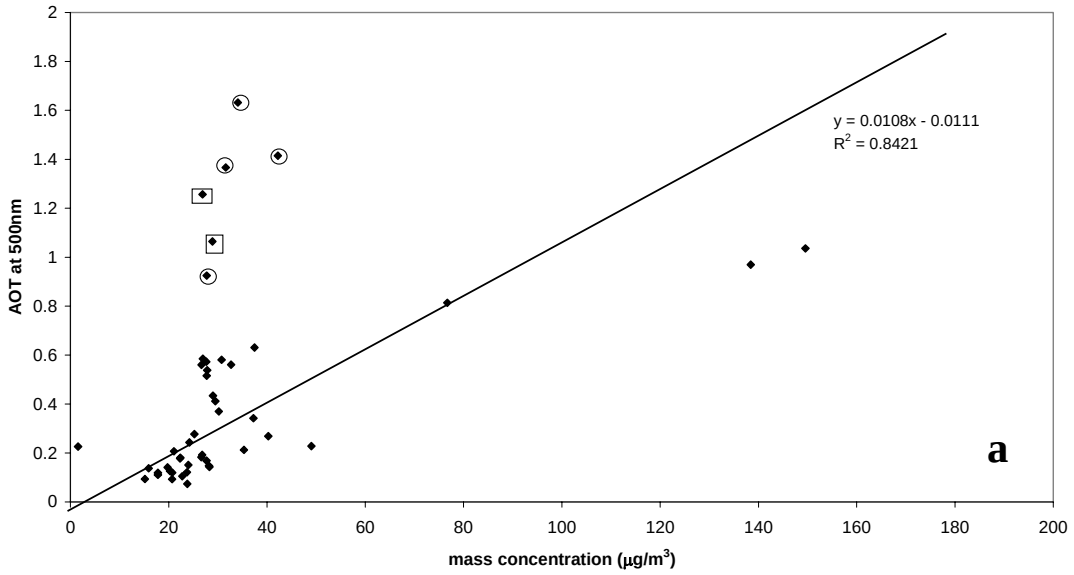

640

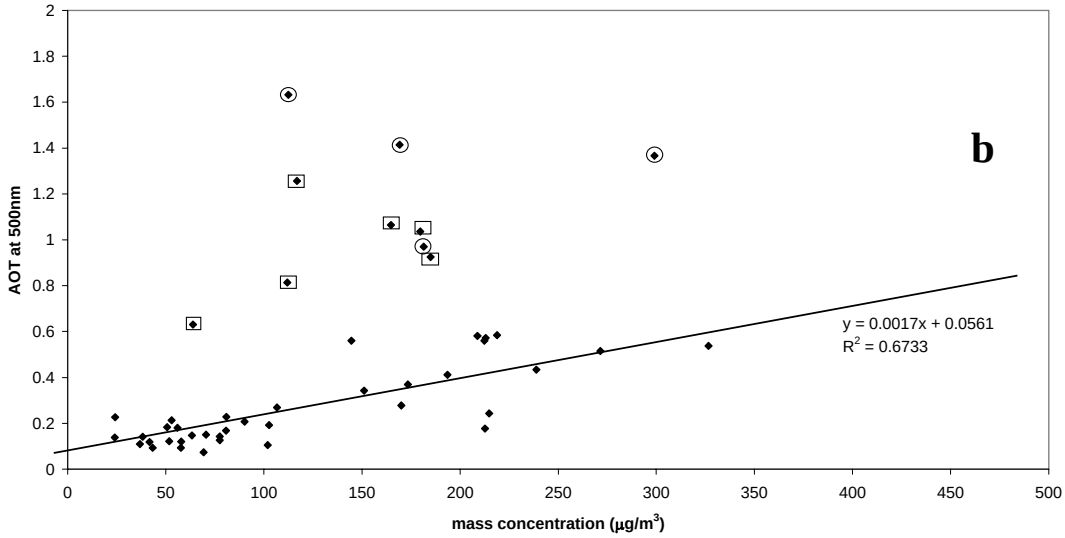

641
642

643 Figure 5. a) Fine mode and b) PM10 concentrations versus AERONET AOT at 500nm.

644 The marked points are not included in the correlation; circled points indicate lack of

645 agreement from the SMR comparison in figure 3 while squared points indicate lack of

646 AERONET size distribution data.

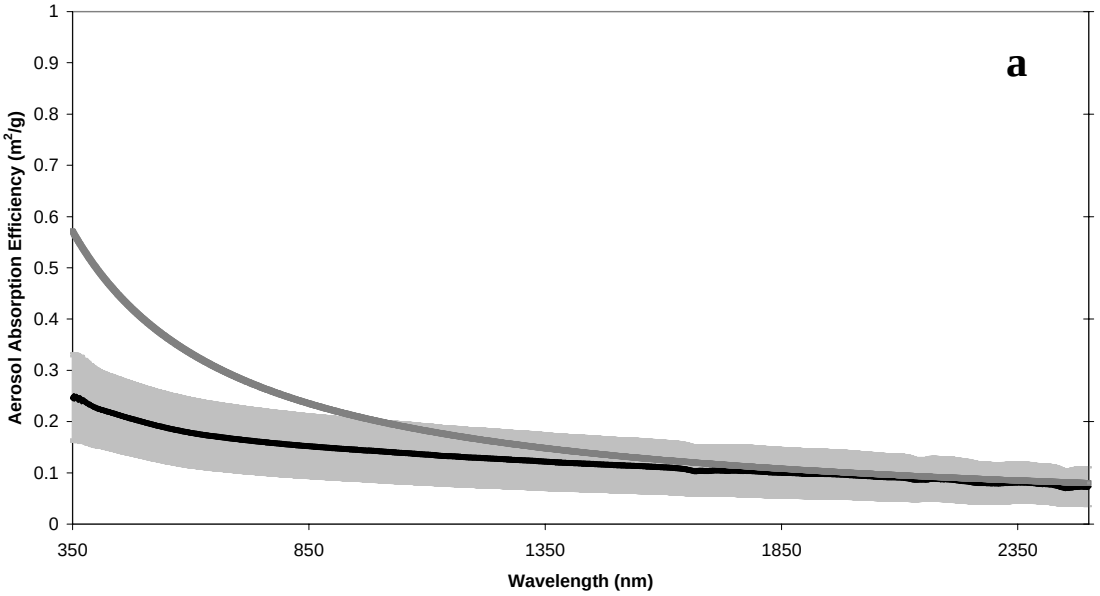
a
Aerosol Absorption Efficiency (m²/g)
1
0.9
0.8
0.7
0.6
0.5
0.4
0.3
0.2
0.1
0
350
850
1350
1850
2350
Wavelength (nm)

647

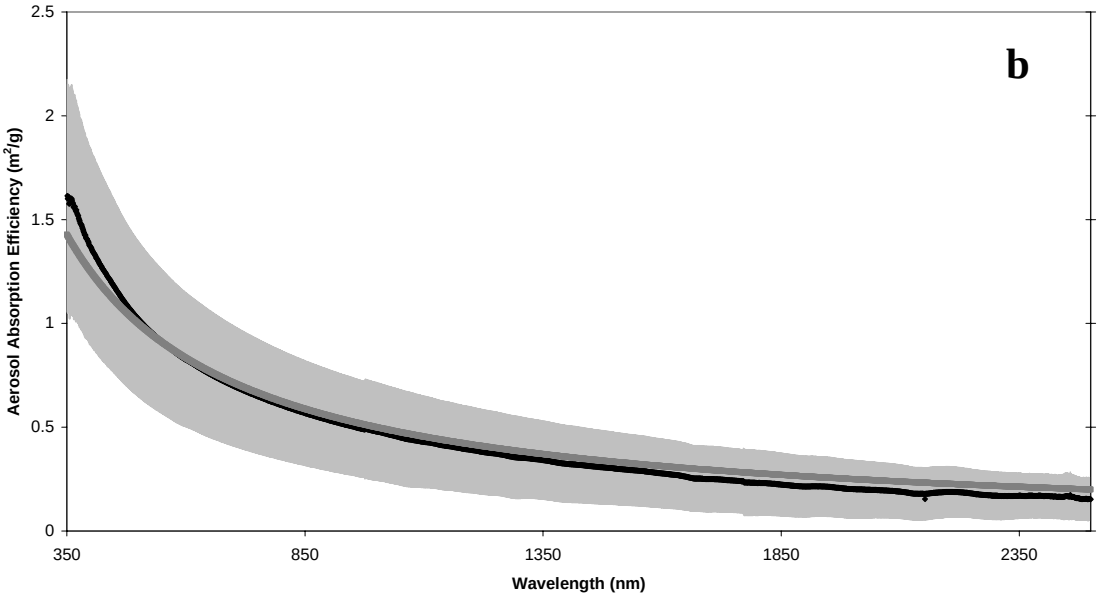
b
Aerosol Absorption Efficiency (m²/g)
2.5
2
1.5
1
0.5
0
350
850
1350
1850
2350
Wavelength (nm)

648

649

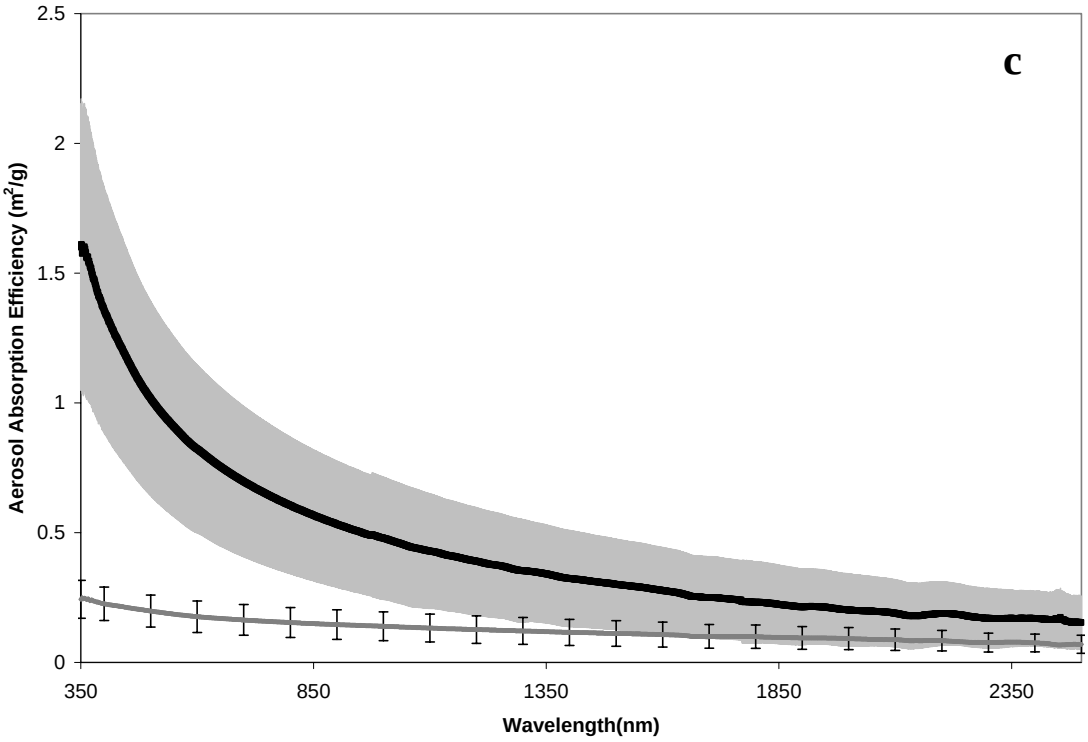

650

651 Figure 6. Spectral Absorption Efficiency for aerosol particles of a) 2.5μm<d<10μm and
652 b) d<2.5μm averaged from 35 filters from March 3-19, 2005 compared to a λ^{-1} model,
653 then compared to each other in c. The gray area in each case represents the standard
654 deviation of the measured cases. The error bars in figure c is equivalent to the gray areas
655 in the figure a plot, but is shown as error bars for visual clarity.

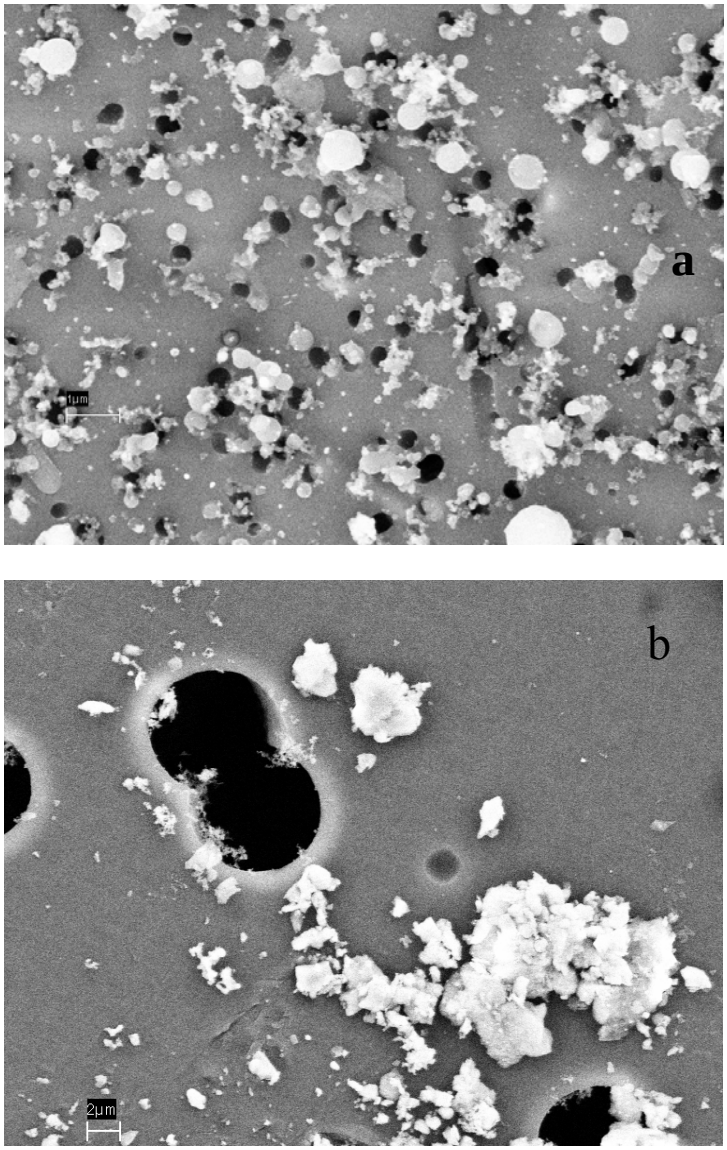

Figure 7. Scanning Electron Microscope image of a) March 10, 2005 fine mode filter and b) March 12, 2005 coarse mode filter. The scale in figure a corresponds to 1µm and the scale in figure b corresponds to 2µm. The black circles shown are the filter pores whereas the particles are shown in white and gray tones.

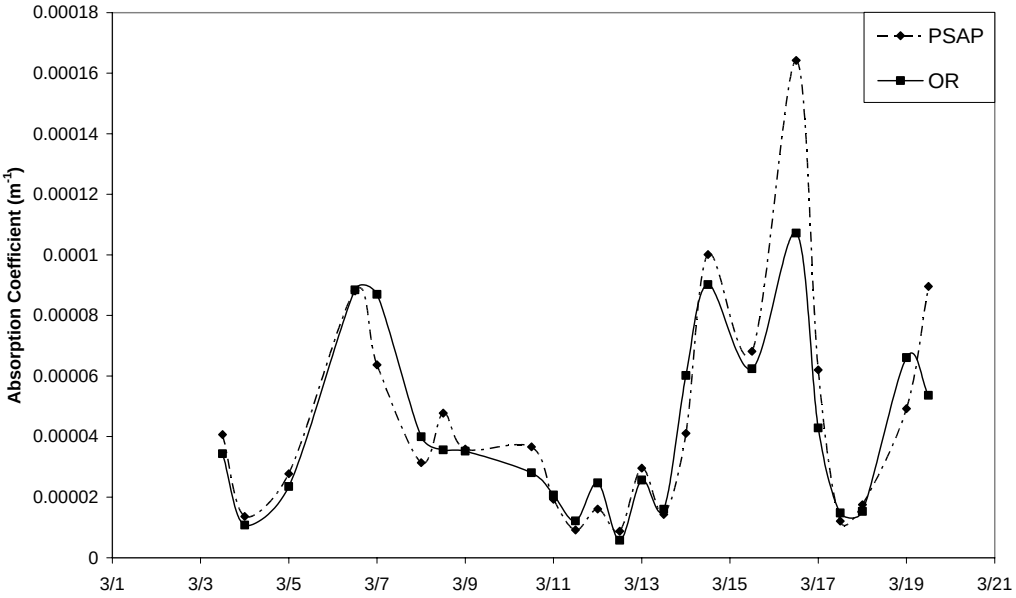

662

663 Figure 8. Comparison of absorption coefficient from the Optical Reflectance (OR)

664 technique applied to the Nuclepore filters and the corresponding average PSAP results

665 during the IOP.

666

667

668

669

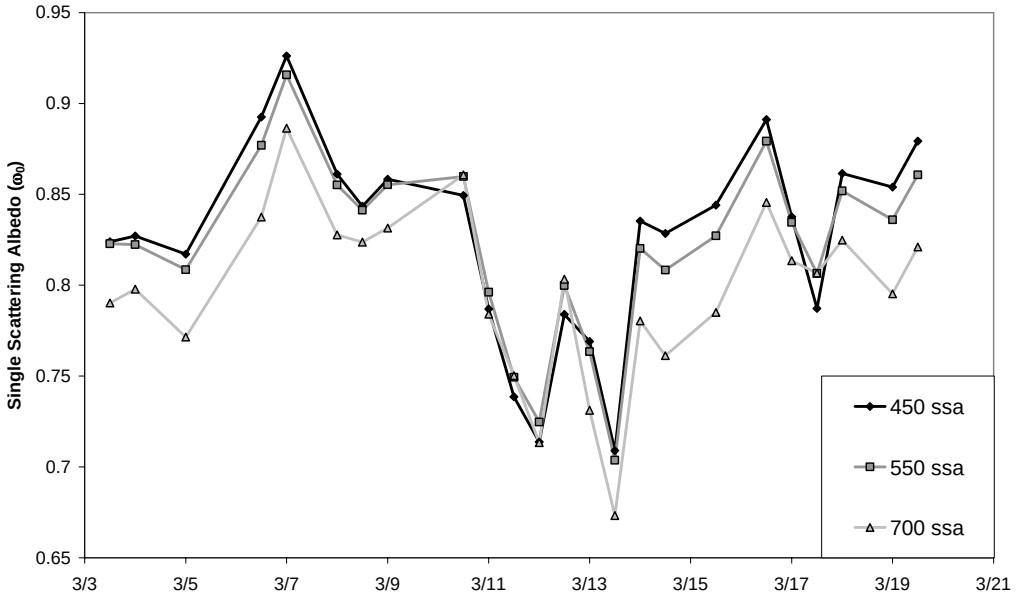

670

671 Figure 9. Single Scattering Albedo (ω_0) from Optical Reflectance combined with the

672 Nephelometer scattering coefficient at the three operating wavelengths: 450, 550, 700nm.

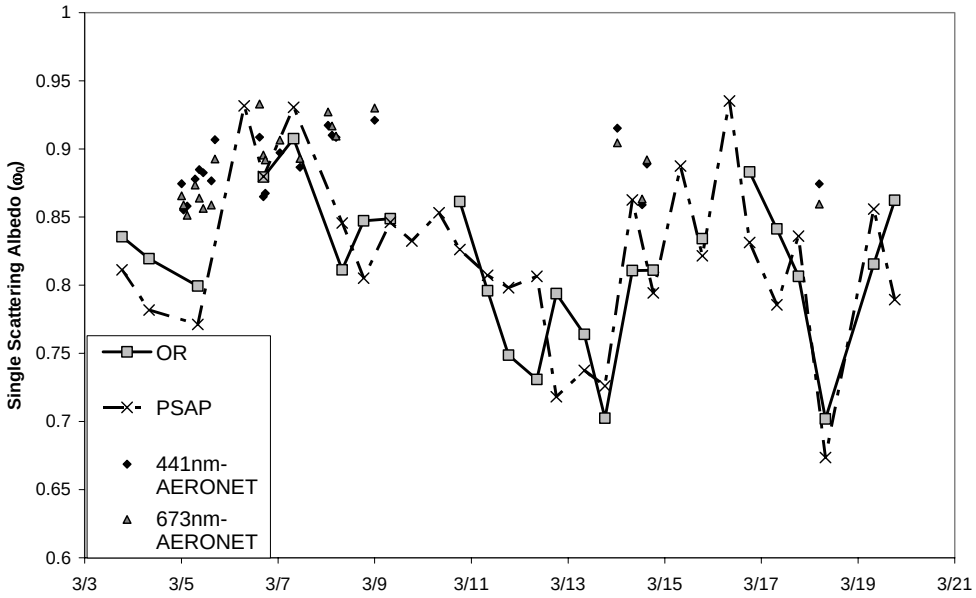

673

674 Figure 10. Single Scattering Albedo from AERONET and a combination of the scattering

675 coefficient from the Nephelometer at 550nm with Optical Reflectance and PSAP results.

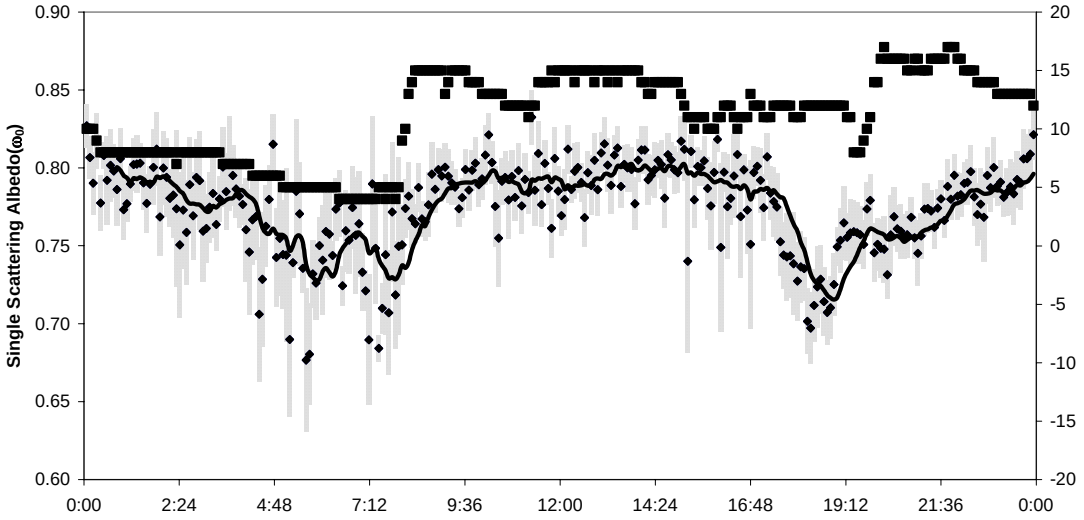

676
677 Figure 11. Diurnal cycle of Single Scattering Albedo from PSAP and Nephelometer with
678 error bars (light gray) and the number of data points from PSAP contributing to the
679 average (squares).